Physics – Uspekhi **45** (12) 1203 – 1211 (2002)

REVIEWS OF TOPICAL PROBLEMS PACS numbers: 61.50.Ah, 61.50.Ks, 61.66.Bi

'Weird' crystal structures of elements at high pressure

T N Kolobyanina

DOI: 10.1070/PU2002v045n12ABEH001186

Contents

Abstract. New crystal structures, in particular incommensurate composite crystals, discovered in the high-pressure phases of Group I, II, IV, and V elements are described, and their intermetallic and other binary structural analogs are discussed.

1. Introduction

Pressure has a strong effect on the properties of solids. Compression markedly changes distances between the atoms and leads to changes in the physical properties, in the nature of the interactions in the crystal, and in the crystal structure proper. The interrelationship of these phenomena constitutes the subject of high-pressure studies.

Knowledge of the crystal structure of high-pressure phases makes the theoretical analysis of the physical properties of solids and stability much easier because, even with modern methods of calculating the free energies of the competing phases, the difference in these energies is comparable to the calculation error.

For a long time, in analyzing the laws governing the transformations of a crystal structure under pressure, it was commonly assumed that a crystal is a collection of more or less closely packed spheres.[1] The density of each subsequent (in pressure) phase must be greater than that of the previous phase. It was assumed that as the substance is compressed, the phase transformation must raise the symmetry and, at the same time, increase the number of neighboring atoms (the coordination number, or CN) up to 12, i.e., lead to the densest packings (a triple-layer fcc structure or an ideal double-layer hexagonal structure). This model has provided a fairly good description of the polymorphism of elements and simple compounds, provided that the compression was comparatively low. A fairly complete picture of the phase transformations in elements can be obtained from handbooks (e.g., see Refs [1, 2]). However, as the range of pressures available for investigation broadens, certain deviations from the established rules emerge. X-ray diffraction from high-pressure phases of Group I, II, IV, and V elements has clearly revealed a reduction in symmetry and packing density in the series of polymorphic transformations. For a long time, some diffraction patterns could not be properly interpreted simply because of their complexity and the lack of sufficiently accurate experimental data.

In modern X-ray diffraction experiments conducted under high pressure, a polycrystalline sample to be studied is placed between diamond anvils, which are relatively transparent for X-ray radiation. The volume of the irradiated substance is about $10^{-3}-10^{-5}$ mm^3. Solving the problem of more complicated structures became possible after the radiation intensity was significantly increased and new, highly accurate methods of diffraction recording [3] were used. The resolving power attained in these studies and the accuracy of measurements of the reflection intensities made it possible to use, in solving structural problems, methods of full-profile analysis of the diffraction pattern, which are based on the method proposed by Rietveld [4]. After additional or new data had been gathered, the structures of a number of high-pressure phases of alkali and alkaline-earth elements and corresponding isostructural phases of Group IV and V elements were determined.

It was found that the new complex structures of high-pressure phases are not to be found among structures of elements under normal conditions. Their analogs can often be found among intermetallic compounds, while some high-pressure phases can be classified as composite crystal structures consisting of two interpenetrating substructures with incommensurate translational periods (in one of the crystallographic directions), which is uncharacteristic of structures of elements under normal pressure.

[1] The packing fraction, or the space-filling factor, is defined as the ratio of the volume of spheres filling a certain volume (say, a unit cell) to the observed volume of this cell.

T N Kolobyanina L F Vereshchagin Institute for High Pressure Physics, Russian Academy of Sciences,
42190 Troitsk, Moscow Region, Russian Federation
Tel. (7-095) 334 07 33. Fax (7-095) 334 00 12
E-mail: tnk@hppi.troitsk.ru

Received 24 January 2002
Uspekhi Fizicheskikh Nauk **172** (12) 1361 – 1369 (2002)
Translated by E Yankovsky; edited by S N Gorin

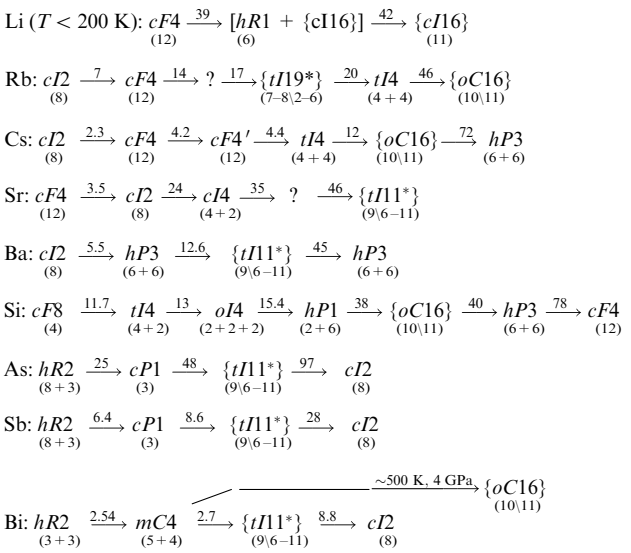

Figure 1. Series of polymorphic transformations of elements under pressure. The new structures are placed inside braces, while the incommensurate composite phases are denoted by an asterisk. The numbers in parentheses under the notation of a structure type correspond to the number of nearest neighboring atoms within the first coordination shell, while the numbers above the arrows indicate the pressure (in GPa) of the corresponding transition. The diagram has been built according to data from the following papers: Li [10, 11]; Rb [12 – 18]; Cs [19 – 22]; Sr [23 – 25]; Ba [23, 26 – 28]; Si [29 – 33]; As [34 – 36]; Sb [37 – 39]; and Bi [39 – 41].

The series of polymorphic transformations of elements, which under pressure form phases with an extraordinary crystal structure, are shown in Fig. 1 (the data have been taken from Refs [10 – 41]). In writing the formulas for structure types, we use the recommendations of the International Union of Pure and Applied Chemistry (IUPAC) [5] to follow the rules proposed by Pearson [2] [6]. For instance, in Rb and Cs, after the bcc structure $cI2$ transformed into the fcc structure $cF4$, with the coordination number increased from 8 to 12, a further increase in pressure revealed the presence of phases with a body-centered tetragonal structure $tI4$ and CN = 8; in Sr, the high-symmetry close-packed fcc structure $cF4$ with CN = 12 transforms under pressure into a looser bcc structure $cI2$ with CN = 8; in Si, the high-symmetry cubic diamond-type structure $cF8$ becomes transformed into a less symmetric but more closely packed tetragonal structure $tI2$ of the white tin type; and, finally, in Bi, the rhombohedral structure $hR2$ transforms into a monoclinic structure $mC4$, with the symmetry lowering in the process.

The lowering of the symmetry and packing density and the emergence of complex structures in high-pressure phases of Group I and II elements are related to the transition, under high pressure, of valence s electrons into the d or p band. The electrons partially occupy orbitals directed into the space between atoms, which leads to a reduction of the charge density on the nucleus and to the loss of spherical symmetry by the atoms and, in the final analysis, to the emergence of complex structures.

Note that in the early 1970s a group of theoreticians headed by Yu Kagan [7, 8] predicted the possibility of the existence of low-symmetry complex structures in monatomic metals. While studying the hypothetical metallic phase of hydrogen via perturbation-theory expansions up to the fourth order in electron – proton interaction, they found that simple cubic and hexagonal structures are dynamically unstable up to extremely high pressures of order 2000 GPa, i.e., within a range of pressures where, according to estimates, hydrogen is sure to exhibit metallic properties. Recently, these results have been corroborated by first-principles calculations [9] based on the density-functional method.

2. New structures of alkali metals and the corresponding isostructural phases of silicon, bismuth, and bismuth alloys

For a long time, alkali metals were interpreted as 'simple metals' with nondirectional metallic bonds. Under normal conditions, these elements (from Li to Cs) crystallize into the bcc structure $cI2$, which is characteristic of metals with nearly-free electrons. As the pressure increases, all these elements except sodium undergo a polymorphic transformation into the fcc structure $cF4$, with the number of nearest neighbors increasing from 8 to 12 and, correspondingly, the packing fraction increasing to the maximum value possible from the viewpoint of sphere packing. Under compression of Rb to 0.3 and Cs to 0.4 of the initial volume, phases with a lower symmetry emerge.

2.1 The *cI*16 structure

X-ray studies conducted by Hanfland et al. [11] have shown that, at pressures above 39.8 GPa and temperatures below 200 K,[3] fcc Li (the $cF4$ structure) passing through the intermediate rhombohedral phase $hR1$ crystallizes in the bcc lattice $cI16$ (space group $I\bar{4}3d$). At 39.8 GPa, $a = 5.272$ Å and the compression ratio $V/V_0 = 0.423$. The atoms occupy the positions 16c on threefold axes, and the positional parameter u grows from 0.045 at 37 GPa and 100 K[4] to 0.06 at 50 GPa. The projection of the structure on the (001) plane in shown in Fig. 2a. The atoms are joined in chains of the

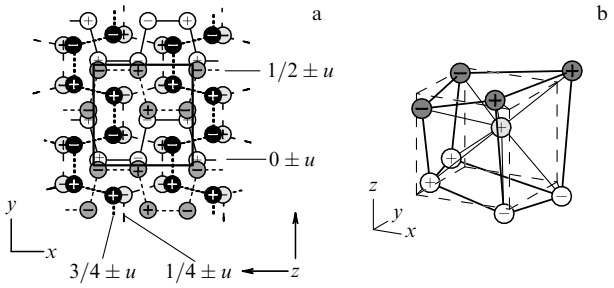

Figure 2. Structure $cI16$: (a) projection of the structure along [001], with circled + and − denoting the displacements of atoms by u from the particular positions 0, 1/4, 1/2, and 3/4; (b) one-eighth of a unit cell, with the dashed lines forming a regular cube.

[2] In a formula for a structure type, the first letter denotes the type of the crystal system (a stands for triclinic (anorthic), m for monoclinic, o for orthorhombic, t for tetragonal, c for cubic, and h for hexagonal), the second letter designates the type of lattice (P stands for primitive, R for rhombohedral, F for face-centered, I for body-centered, and C for base-centered; actually, this is the first letter in the notation for the space group), and the number indicates the number of atoms in the unit cell.

[3] The experiments were conducted at a low temperature to avoid the corroding effect of lithium on the diamond anvils at pressures above 20 GPa [10, 11].

[4] This point was obtained in the cycle of a pressure decrease [11].

Table 1. Parameters of the *oC*16 structure for high-pressure phases Rb VI, Cs V, Si VI, and Bi IV and alloys $Bi_{0.8}Pb_{0.2}$ and $Bi_{0.7}In_{0.3}$.

Phase	Rb VI 48.1 GPa	Cs V 25.8 GPa	Si VI 42.5 GPa	Bi IV 3.96 GPa 503 K	$Bi_{0.8}Pb_{0.2}$ −190 °C	$Bi_{0.7}In_{0.3}$ −190 °C
a, Å	9.372	10.641	7.968	11.121	11.109	11.236
b, Å	5.550	6.278	4.776	6.580	6.672	6.555
c, Å	5.528	6.249	4.755	6.580	6.658	6.531
V_{at}, Å^3	17.970	26.090	11.308	30.090	31.12	30.07
y (8f)	0.170	0.188	0.172	0.173	0.172	0.170
z (8f)	0.318	0.328	0.328	0.327	0.328	0.330
x (8d)	0.211	0.217	0.219	0.216	0.214	0.212
V/V_0	0.194	0.226	0.566	0.850		
a/c	1.689	1.699	1.672	1.690	1.684	1.721
b/c	1.004	1.005	1.005	∼ 1	1.002	1.004
References	[18]	[21]	[33]	[41]	[41]	[41]

meander type extending along the coordinate axes. The transverse sections of the meander are alternatively lowered and raised by u in relation to the planes with $z = 0$, 1/4, 1/2, and 3/4.

The *cI*16 cell may be thought of as consisting of eight deformed cells of the body-centered structure *cI*2. Each atom has three nearest neighbors 2.174 Å apart in its chains, while in the neighboring chains there are two next-nearest neighbors 2.28 Å apart and six next-nearest neighbors 2.40 Å apart. Thus, CN = 3 + 2 + 6 = 11, i.e., the structure remains fairly close-packed.

Calculations of the electron density of states [11] for a compression ratio $V/V_0 = 0.4$ (theoretical pressure amounting to 48.8 GPa) show that when the symmetry of the structure is lowered to *cI*16, there is a considerable reduction in the density of states at the Fermi level and an increase in the maximum density of states directly below the Fermi level caused by the filling of the 2p band. Here, the total electron energy is reduced compared to the energies in the superlattice *cI*16 at $u = 0$ and also in the *hR*1 and *cF*4 lattices (Fig. 3). The results of electron density calculations have revealed the presence of substantial peaks in the charge density in the interatomic spaces inside the chains and between the chains.

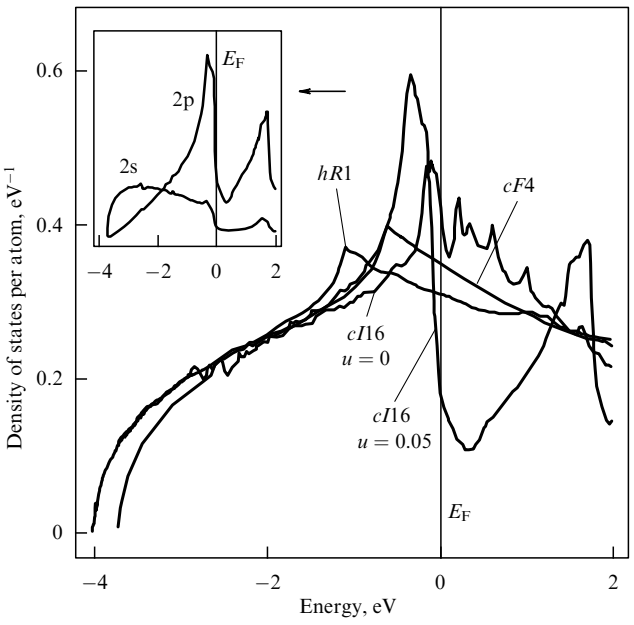

Figure 3. Electron density of states in Li for a compression ratio $V/V_0 = 0.4$ calculated for the structures *cF*4, *hR*1, and *cI*16 ($u = 0$ and $u = 0.05$). The data have been taken from Ref. [11].

2.2 The *oC*16 structure

Historically, the first structure to be solved was that of the Cs V phase [21], which exists in a pressure range from 12 to 72 GPa [22]. Cs V crystallizes in the space group *Cmca* with 16 atoms per cell, and the structure type is *oC*16. Later it was found that the same structure is characteristic of the phases Rb VI above 48 GPa [18] and Si VI in a range of 38 – 49 GPa [33], the high-temperature phase Bi VI in the vicinity of 40 GPa and 500 K, and the alloys $Bi_{0.8}Pb_{0.2}$ and $Bi_{0.7}In_{0.3}$ obtained by compression to 2 GPa and heating to 100 °C followed by cooling to liquid-nitrogen temperatures and by relieving the pressure (X-ray recording is also done at low temperatures) [41]. The data on the structure of these phases are listed in Table 1. Note the almost perfect similarity of the structures of the different representatives: the axial ratios and positional parameters of the atoms are the same. These quantities remain virtually the same under changes in pressure, too.

In the space group *Cmca*, the atoms of the *oC*16 structure occupy two independent types of positions: the positions 8*f* in the symmetry planes (*a*1), and the positions 8*d* on the twofold axes (*a*2). The *a*1 atoms form two 3^2434 nets[5] shifted by $\mathbf{a}/2 + \mathbf{b}/2$ relative to each other; these nets alternate with corrugated nets $\sim 4^4$ consisting of *a*2 atoms (Fig. 4a). Strictly speaking, following Pearson's rules, the latter should have been depicted by two crossed flat grids 4^4. However, the level of corrugation ($\pm 0.032a$) is not large, and depicting a layer consisting of only one net makes perception of the mutual

[5] Here we use the representation (proposed by Pearson [6]) of structures produced by superimposing (or overlapping) nets formed by connecting the nearest atoms of a planar layer by straight line segments. The notation of a network is built around a circular traversal of a site: 3 stands for a triangle, 3^2 for two triangles in succession, 4 for a square, 5 for a pentagon, etc.; for instance, a close-packed hexagonal layer is characterized by the net 3^6, and a graphite-like layer by 6^3.

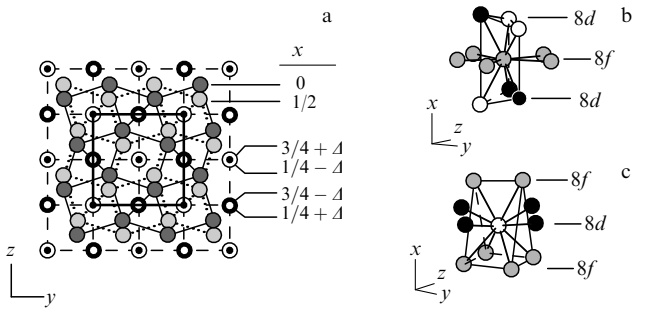

Figure 4. Structure *oC*16: (a) 3^2434 nets consisting of 8*f* atoms and $\sim 4^4$ nets consisting of 8*d* atoms in the projection along [100], $\Delta = 0.032$; (b) coordination of 8*f* atoms, CN = 11; and (c) coordination of 8*d* atoms, CN = 10.

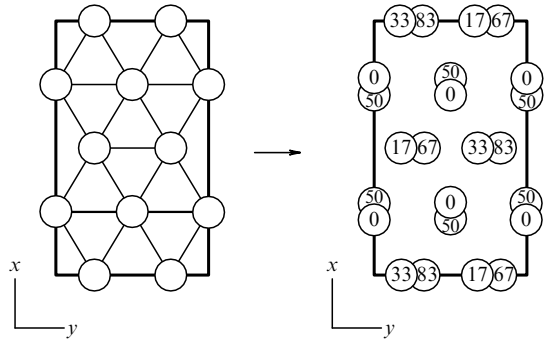

Figure 5. Transition from the *hP*1 structure to the *oC*16 structure in the setting *Cmca*, with the projection being along [001]; the numbers in circles stands for hundredths of the parameter *z*.

arrangement of atoms easier. The atoms *a*1 (8*f*), as notation 3^2434 shows, have five nearest neighbors in their own layer, with one distance being the shortest in the structure. Each *a*1 atom is inside a deformed trigonal prism consisting of *a*2 atoms and has four nearest neighbors at equal distances and two more neighbors at somewhat greater distances (Fig. 4b). The coordination of the *a*1 atoms is $5(a1) + 6(a2)$. The atoms *a*2 (8*d*) are surrounded by four nearest neighbors located at approximately equal distances in their own layer; each of these atoms is inside a distorted trigonal prism consisting of *a*1 atoms (Fig. 4c). Chains of prisms (consisting of *a*1 atoms that are connected by almost square faces and have edges that are the shortest distances in the 3^2434 net) propagate along the **a** axis and fill the entire space. The coordination number for the *a*2 atoms is $4(a2) + 6(a1)$. Thus, in the *oC*16 structure, the atoms that occupy different crystallographic positions have different coordination numbers: 11 for 8*f* atoms, and 10 for 8*d* atoms.

The *oC*16 structure can be obtained from the body-centered tetragonal structure *tI*2 or the fcc structure *cF*4 by rotating the squares consisting of *a*1 atoms about the chains consisting of *a*2 atoms [21]. However, the Rb V and Cs IV phases, which precede the *oC*16 phase in pressure, have a body-centered tetragonal structure *tI*4 (the space group $I4_1/amd$) with an axial ratio $c/a = 3.73$ and CN = 8 [16, 20]. The *tI*4 structure is obtained by adding two *tI*2 structures shifted by $\mathbf{a}/2 + \mathbf{c}/4$ relative to each other. The same structure can be represented in the form of four nets 4^4 separated by distances equal to $c/4$ and shifted, respectively, by $\mathbf{a}/2$, $\mathbf{a}/2 + \mathbf{b}/2$, and $\mathbf{b}/2$ relative to the net with $z = 0$. The transition from *tI*4 to *tI*2 can be achieved through a shift of the nets with $z = 0$ and $z = 1/2$ along [110] toward each other by one-fourth of a translation along this direction, and a shift of the lattices with $z = 1/4$ and $z = 3/4$ by the same amount toward each other along $[1\bar{1}0]$. Thus, the *cF*4, *tI*2, *tI*4, and *oC*16 structures can be obtained from each other via small deformations, shifts, and rotations. The last known phase Cs VI crystallizes into a hexagonal close-packed or double hexagonal close-packed structure [22] with CN = 6 + 6.

In silicon, the preceding (in pressure) phase Si V has a simple hexagonal structure *hP*1 with $c/a = 0.944$ and CN = 2 + 6, while the phase Si VII, following *oC*16, has a hexagonal close-packed structure *hP*2 with $c/a = 1.699$ and CN = 6 + 6 [29], which under further compression transforms into an fcc structure *cF*4 with CN = 12 [30]. The *hP*1 structure can be represented in the *Cmca* setting if the atoms 8*f* and 8*d* occupy certain particular positions (Fig. 5) and the lattice parameters meet the following condition: $b_o/a_o = 1/\sqrt{3}$; then $c_h = c_o/2$ and $a_h = a_o/4 = b_o/2$ [33].

The *hP*2 structure can be obtained by prolonging the tendency of changes in the coordinates in the *Cmca* setting:

		*hP*1	*oC*16	*hP*2
8*f*:	$y =$	0.25	0.173	0.125
	$z =$	0.5	0.328	0.25
8*d*:	$x =$	0.25	0.224	0.25

The 8*d* atoms arrange themselves to match the close-packed layer of 8*f* atoms via small shifts $\Delta y = 1/8$ in chains with $z = 0$ and $\Delta y = -1/8$ in chains with $z = 1/2$; the value of z changes by $\Delta z = -1/12$ (Fig. 6). Then $c_h = a_o/2$ and $a_h = b_o/2$ provided that $c_o/b_o = \sqrt{3}/2 = 0.866$. The leading role of the net of 8*f* atoms in the transformation of *oC*16 into *hP*2 is emphasized by the fact that the average distance between the nearest atoms in the 3^2434 net is almost equal to a_h in *hP*2.

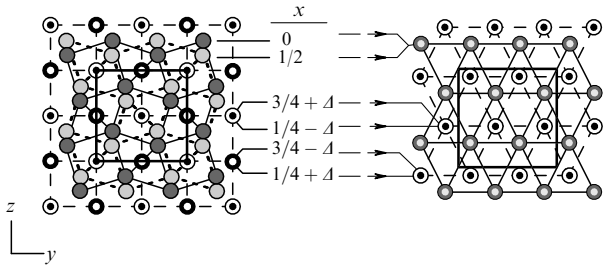

Figure 6. Transition from the *oC*16 structure to the *hP*2 structure in the *Cmca* setting, with the projection being along [001].

Thus, as in Cs and Rb, the *oC*16 structure in Si can be obtained from the structures of the neighboring phases by lowering the symmetry via small variations of the positions of the atoms and is an intermediate structure between structures with CN = 8 and CN = 12.

The stability of the *oC*16 structure in Cs and Si in relation to the structures of the neighboring phases has been demonstrated by the theoretical calculations of Ahuja et al. [42, 43]. Chang and Cohen [44] found that in Si, as pressure forces the atoms to move closer to each other, the valence sp electrons become nearly free already in the *hP*1 phase. In Cs, the structural stability depends on the occupancy of the d

band. Changes in the band structure, the density of states, and the electron density of cesium, examined as functions of the volume, have been analyzed within the framework of the *cF*4 structure by Louie and Cohen [45]. The results of the calculations show that, as the pressure increases, the d-band energy decreases, the density of d states below the Fermi level increases because of the drop of the density of s states, the electron density loses its spherical symmetry with respect to the point where the Cs atom is, and the charge is drained away, so to say, from the atom into the space between the nearest atoms, forming local maxima there; Cs becomes a d transition metal. McMahan [46] found through calculations that the $s \rightarrow d$ transition in Cs is terminated when the compression-induced volume change reaches $V/V_0 = 0.235$, which approximately corresponds to a pressure of 22 GPa [21], that is, long before the next transition from *oC*16 to the hexagonal structure existing at 72 GPa occurs. Detailed calculations of the band structure, the density of states, and the electron density of Si and Cs in the *oC*16 structure done by Schwarz et al. [47] revealed that the interactions in these elements have opposite origins. In Si, the band structure and the density of states correspond to the behavior of nearly free electrons; the charge density of the valence electrons exhibits significant peaks between the nearest neighbors in the 3^2434 and $\sim 4^4$ nets, which is characteristic of covalent interaction. In Cs, on the other hand, the buildup of charge, caused by the contribution of d orbitals of different symmetries of all the neighboring atoms, occurs primarily at the centers of the squares of the nets; the energy bands corresponding to such interaction are the deepest; and the density of states below the Fermi level has two distinct d maxima, which corroborates a conclusion drawn from earlier calculations that under pressure cesium becomes a d transition metal.

2.3 The *tI*20 or the *tI*19 structure?

The existence of the Rb IV phase in the range of 17 – 20 GPa has been established by several methods, including the X-ray diffraction method [13]. New X-ray experiments have led to the discovery of a surprisingly complex structure with a large tetragonal cell [14]. Under a pressure of 16.9 GPa, the cell parameters are $a = 10.357$ Å and $c = 5.184$ Å; $c/a = 0.5005$ and increases with pressure. Extrapolating the pressure dependences of atomic volumes in the phases Rb II (*cF*4) and Rb V (*tI*4) into the region of existence of the phase Rb IV, the researchers found that the number Z of atoms in a unit cell varies from 18.5 to 20. The use of direct methods for solving the structure in the space group $I4/mcm$ has shown that some of the Rb1 atoms occupy the positions 16*k* in the mirror-reflection planes with coordinates $x = 0.792$, $y = 0.084$ and form two 48^2 nets rotated by 90° in relation to each other (Fig. 7a). The structure consists of columns (arranged parallel to the **c** axis) of square antiprisms (Fig. 7b) placed in the corners and at the center of the unit cell (Fig. 7a). The columns are 3.04 Å apart from one another (this is the shortest distance in the structure). As a result, along the faces of the unit cell that are parallel to the *c* axis, there are rather wide channels formed by crossed elongated octagons, into which approximately four more Rb2 atoms must be placed. The electron density calculated from the intensities suggests that there are two possible variants of arrangement of Rb2 atoms in linear chains along twofold axes: in positions 4*b* or 8*g* with half occupancy (Fig. 7c). This means that the Rb2 atoms occupy positions on the cell faces that are parallel to the *c* axis at heights that are either $z = 1/4$ and $z = 3/4$ (4*b*) or

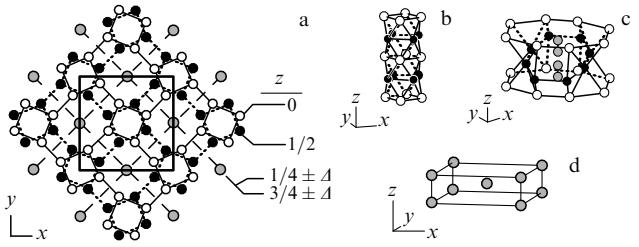

Figure 7. Structures *tI*20 and *tI*19: (a) projection of the structure along [001], $\Delta = 0.11$; (b) a column of square antiprisms of 16*k* atoms; (c) arrangement of 8*g* atoms in channels of 16*k* atoms in the *tI*20 structure; and (d) incommensurate body-centered tetragonal substructure in the *tI*19 structure.

$z = 1/4 \pm \Delta$ and $z = 3/4 \pm \Delta$ (8*g*), where $\Delta = 0.11$. Here, the average distance between atoms in a chain is 2.59 Å, which is 15% smaller than the diameter of the Rb ion. The researchers believe that the half-occupancy of the positions 8*g* provides an optimum description of the *average* arrangement of the Rb2 atoms. Within this approach, the coordination of the atoms amounts to the following for Rb1: 1×3.04 Å $+ 2 \times 3.31$ Å in a layer; 4×3.15 Å between the layers; and 1×3.46 Å with Rb2, so that *in toto* CN = 7(Rb1) + 1(Rb2) = 8; for Rb2 we have 2×2.59 Å in the chains and 8×3.46 Å with Rb1, so that *in toto* CN = 2(Rb2) + 8(Rb1) = 10. The case of simultaneous occupancy of positions 4*b* with a probability equal to 0.17 and positions 8*g* with a probability equal to 0.35 was also examined, which led to more reasonable values of the average distance in the chains, 2.97 Å, and of the number of atoms per cell, $Z = 19.48$, but such a result is not justified by the accuracy of the experiment. However, if we turn to the variant of occupancy of the positions 8*g* with a probability equal to 0.5, which is considered to be an optimum variant, we notice that the Rb2 atoms must occupy, with a probability equal to 0.25, positions with $z = 1/4 + \Delta$ and $z = 3/4 - \Delta$ separated by a distance of 1.45 Å, which is practically impossible, with the result that the formation of vacancies and the accompanying reduction in the number of atoms per cell seem to be inevitable.

Indeed, on the basis of new experimental data, McMahon et al. [15] concluded that the atoms in the channels of the first basic structure form their own substructure with an incommensurate translation in the direction **c**. These researchers were able to obtain single-phase Rb IV in a range of 17 – 16.5 GPa under pressure reduction. Here, the diffraction pattern clearly revealed reflections that could not be indexed in the framework of the basic lattice $I4/mcm$. They are indexed on the basis of a body-centered tetragonal cell with a space group $I4/mmm$ and have the same parameter *a* as in the first cell, but the parameter *c* is smaller by a factor of 1.627 than that in the first cell (Fig. 7d). At 16.8 GPa, the parameters have the values $a_I = a_{II} = 10.3503$ Å, $c_I = 5.1865$ Å, and $c_{II} = 3.1797$ Å, and the number of atoms per cell of the basic substructure is $Z = 19.262$. The coordination of the Rb1 atoms is as follows: 1×3.04 Å $+ 2 \times 3.31$ Å $+ 4 \times 3.15$ Å with Rb1, and 1×3.147 Å with Rb2 if Rb1 and Rb2 are in the same plane; the coordination of the Rb2 atoms is as follows: 2×3.18 Å in chains of Rb2, and 4×3.147 Å with Rb1 if the atoms are in the same plane. The c_I/c_{II} increases with pressure, i.e., in the direction [001] the framework structure is more rigid than the embedded

structure. Thus, the flaw in the previous solution of the structure, the distance between the atoms in chains being too short, is removed. Here, it is equal to 3.18 Å, which is greater than the shortest distance of 3.04 Å in the basic substructure. And, indeed, the number of atoms per cell decreases.

3. Incommensurate structures of heavy alkaline-earth elements and Group V elements

Under normal conditions, strontium crystallizes in the *cF*4 structure and at 3.5 GPa the structure becomes *cI*2; then, as the pressure increases, strontium undergoes a number of phase transitions accompanied by a lowering of symmetry; the transition to the Sr V phase occurs at 46 GPa [23–25]. Refinement of the phase diagram for barium showed that after the transition Ba I ($cI2$) → Ba II ($hP2$) at 12 GPa is completed, there occurs a transition to the Ba IV phase with a structure of reduced symmetry, and then, at 42 GPa, to the Ba V phase with an $hP2$ structure. Comparison of the temperature variations of the pressure dependence of the axial ratio c/a in Ba II with the value of c/a in Ba V suggests that this is a single phase encompassing the Ba IV phase from the high-temperature side [26]. The phases Sr V and Ba IV are isostructural [23]. The structures of Sr V [25] and Ba IV [28] have been solved on the basis of new diffraction data obtained from polycrystalline samples and from single-crystal grains (monocrystallites) grown in a high-pressure chamber. The lowering of the symmetry that occurs in phase transitions under pressure in heavy alkaline-earth elements is considered to be a manifestation of the electron s → d transition in the crystal structure, just as it is in alkali elements.

Nelmes et al. [28] found that the complex diffraction pattern in Ba IV consists of reflections from several sublattices with incommensurate periods of translations along the fourfold axis of the first basic ('host,' in terms of these researchers) base-centered tetragonal substructure. The space group of substructure I is $I4/mcm$, with the atoms occupying the crystallographic positions 8*h* with $x \cong 0.15$ and forming two 3^2434 nets with $z = 0$ and $z = 1/2$ (Fig. 8a). The nets overlap in such a way that channels consisting of square antiprisms parallel to the **c** axis are formed along the vertical edges and at the center of the unit cell. The channels contain linear chains of atoms of the other two substructures ('guest' substructures) with periods of translation along **c** that are incommensurate with the period of substructure I. Substructure II, described as a base-centered tetragonal structure (Fig. 8b), forms flat 4^4 nets that are parallel to the (001) plane of the first. The chains of atoms are disordered along the **c** axis, which results in intense diffuse scattering from a series of planes in the diffraction pattern of the monocrystallite. This substructure is somewhat more rigid than the host substructure, since the ratio $c_{\rm I}/c_{\rm II}$ decreases with increasing pressure. Some of the weak reflections have been indexed on the basis of four identical *C*-centered monoclinic lattices, which are related through 90° rotations about the fourfold axis and constitute substructure III. This substructure is a monoclinic distortion of substructure II (Fig. 8b) and forms the same nets, which, however, are positioned at an angle to the (001) plane of substructure I. The researchers believe that the monoclinic distortion reduces local stresses generated when the atoms of substructures I and II are too close to each other. At 12.5 GPa, the monoclinic substructure undergoes a phase transformation and becomes an orthorhombic

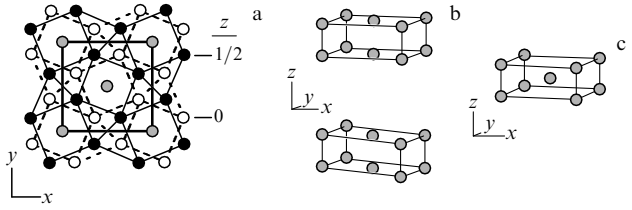

Figure 8. Incommensurate structures *tI*11: (a) superimposition of the 3^2434 nets of the basic (host) substructure and the arrangement of the atoms of the other substructures in channels consisting of square antiprisms of the basic substructure; (b) the base-centered tetragonal and monoclinic substructures; and (c) the body-centered tetragonal substructure.

substructure with the parameters of substructures I and II remaining unchanged. The diffraction pattern of substructure III changes again at 18 GPa. Thus, the Ba IV phase is subdivided into phases IVa, IVb, and IVc. The structural characteristics of the crystal are listed in Table 2.

New diffraction data for Sr V have been gathered by McMahon et al. [25] for pressures ranging from 49 GPa to 74 GPa. The structure of Sr V resembles that of Ba IV almost perfectly, the only difference being that in Sr V there are no monoclinic and orthorhombic substructures. Diffuse scattering from the chains of atoms of substructure II, which are disordered along the **c** axis, manifests itself only as pressure increases, but the researchers have difficulties in determining the reason why such scattering becomes more intense with pressure: is it due to an increase in disorder or an increase in the size of the crystallites? They give the values of the parameters of the crystal structure only for 56 GPa, which makes it impossible to estimate the relative rigidity of substructures I and II in Sr V (see Table 2).

McMahon et al. [39] discovered a similar crystal structure in the high-pressure phases Bi III (2.7–7.7 GPa) and Sb III[6] (above 8.6 GPa). New diffraction measurements of Bi III were conducted at 4.5 GPa with a monocrystallite and at 6.8 GPa with a polycrystal. To solve the structure of Sb III, the data of other researchers [48, 49], obtained at 9.5 GPa and 12 GPa, were used. Substructure I is built from 3^2434 nets in the same way as in the case of Ba IV and Sr V. However, substructure II has a body-centered tetragonal lattice belonging to the space group $I4/mmm$ (see Fig. 8c and Table 2). The diffraction pattern of the Bi III monocrystallite also contains diffuse scattering lines, which indicate that the chains of atoms inside channels formed by antiprisms of substructure I are disordered.

In solving the structure of crystals with incommensurate sublattices under high pressure, there emerges a special problem, namely, that of determining the number of atoms in the unit cell, since there is a strong correlation between two varied quantities — the parameters of the preferred orientation model and the occupancy of the positions in the sublattices [39]. In the structure of Bi IV with a 100% occupancy of the positions 8*h* in the host sublattice, refinement of the structure yields a 100(1)% occupancy in all the other positions, a result that agrees well with the

[6] The researchers denoted the phase of antimony that exists at pressures higher than 8.6 GPa by Sb II. However, the existence of Sb II with a simple cubic structure in the range of 6.4–8.4 GPa under quasi-hydrostatic compression has been established by X-ray analysis (by a photomethod and by diffraction measurements) [37, 38].

Table 2. Incommensurate structures $tI11$ of high-pressure phases in Ba, Sr, Bi, and Sb.

	Ba IVa	Ba IVb	Sr V	Bi III	Sb III	
p, GPa	12.0	12.9	56	6.8	9.5	12
Substructure I, space group $I4/mcm$						
a, Å	8.4207	8.3460	6.958	8.5182	8.032	7.965
c, Å	4.7369	4.6966	3.959	4.1642	3.899	3.858
c/a	0.5625	0.5627	0.569	0.4889	0.485	0.484
x ($8h$)	0.1486		0.146	0.1536		
Substructure II						
Symmetry	Base-centered tetragonal			$I4/mmm$		
a, Å	8.4207	8.3460	6.961	8.5182	8.032	7.965
c, Å	3.4117	3.4095	2.820	3.1800	2.988	2.945
c/a	0.4051	0.4085	0.405	0.3733	0.372	0.370
Substructure III						
Symmetry	Base-centered monoclinic	Orthorhombic				
a, Å	8.4623					
b, Å	8.4207					
c, Å	3.4269	3.4070				
β, °	96.151					
c_I/c_{II}	1.3884	1.3775	1.404	1.3095	1.305	1.310
c_I/c_{III}	1.3823	1.3875				
Z	10.777	10.755	10.808	10.619	10.610	10.620
V/V_0	0.491		0.315	0.83	0.78	
References	[28]	[28]	[25]	[39]	[39]	[39]

pressure dependence of the volumes $V(p)$ in the Ba II and Ba V phases [27]. In Sr V, a well-developed texture present in the sample obstructs the direct determination of the occupancy, and its is assumed to be equal to 100% on the grounds that the relative parameters of the corresponding substructures in Sr V and Ba IV are practically equal [25]. For Bi III, the same occupancy value is in good agreement with the compressibility and the volume discontinuities that occur in II → III and III → V transitions and have been measured by Bridgman's volumetric technique [50]. The volume of Sb III shows considerable disagreement with the magnitude of the volume discontinuity in a transition measured by Bridgman [50]. However, the researchers believe that new diffraction studies will improve the situation.

Lately, it has been established that the As III phase has the same host substructure as Sb III and Bi III but that the chains of atoms located in the channels form an incommensurate body-centered monoclinic lattice with a ratio $c_I/c_{II} = 1.309$ [36].

The Sr V, Bi IV, Bi III, and Sb III phases can truly be classified as composite crystals. A characteristic feature of such crystals is the existence of two or more interpenetrating substructures with incommensurate periods of translation along certain directions. Correspondingly, the diffraction pattern of such a crystal consists of two or more groups of principal reflections from 3D sublattices and weak satellite reflections, which point to modulations of each sublattice that are caused by the interaction between the substructures. The reflection intensity is determined by the diffraction contribution not only from the proper sublattice but also from the second sublattice and by the contribution from the modulations. Hence, it is difficult to accurately determine the structure on the grounds of only principal reflections. The difficulties are resolved if the crystal is examined in $(3 + d)$-dimensional space. The necessary mathematical tools have been developed for both diffraction from a single crystal and diffraction from a polycrystalline sample [51]. For example, fairly recently Bolotina et al. [52] used X-ray diffraction analysis methods in the formalism of $(3 + 1)$-dimensional superspace (supercrystal) to study the composite crystal structure of the modulated $Mg_2Sn_{1.1}$ phase synthesized from a Mg_2Sn melt under a pressure of 5.8 GPa. The monoclinic and orthorhombic substructures in Ba IV are, possibly, a manifestation of the modulations that emerge in the interaction of the incommensurate tetragonal substructures. As is known, in modulated structures the indices of satellite reflections are temperature-dependent [53]. Obviously, if the substructures have different rigidities, this phenomenon can also emerge under pressure variations. Then, the 'phase transitions' in Ba IV may actually prove to be changes in the modulation of the substructures under pressure.

4. Conclusions

The high-pressure phases of elements depicted in Fig. 1 demonstrate the diversity of the manifestations of the

electron transitions in the crystal structure of matter: the isostructural transition in Cs, $cF4 \rightarrow cF4'$; a lowering of the symmetry and the formation of less close-packed structures $hR1$, $cI16$, $tI4$, $oI4$, and $mC4$; and the formation of incommensurate structures $tI19$ and $tI11$ and structures where the atoms occupy different crystallographic positions, $oC16$. This division of atoms into groups in the last three types of structures is an indication that the states of the same atoms in the corresponding high-pressure phases are not the same. Structural analogs of new structures are also to be found only among binary compounds, often intermetallic compounds.

The Li $cI16$ structure corresponds in all aspects to the CoU $cI16$ structure [54], which is a highly distorted structure of the CsCl type with a unit cell constituting a block of eight cells of the CsCl type. The plutonium sublattice of the Pu_2C_3 $cI40$ crystal [55] also exactly reflects the Li $cI16$ structure. The theoretical calculations done by Neaton and Ashcroft [56] have shown that, under compressions somewhat higher than in $cI16$, it is possible to combine two Li atoms into a molecule shaped like a dumbbell. In this phase, lithium should become a semiconductor with a narrow energy gap [56], i.e., under a sufficiently high pressure a metal–insulator transition may take place. This possibility aroused considerable interest among theoreticians and experimentalists [11]. An analog of this hypothetical structure is the structure of the metallic iodine I_2 $oC8$ [57], into which iodine crystallizes under normal conditions. In the $oC8$ structure, one can easily visualize chains of atoms of the meander type characteristic of $cI16$.

The closest analog of the incommensurate structure of Rb $tI19$ is the tungsten sublattice of crystals of the W_5Si_3 $tI32$ compound [58]. In the unit cell of W_5Si_3, 16 atoms of W form two antisymmetric (in relation to each other) 48^2 nets consisting of elongated octagons and squares in the planes $z = 0$ and $1/2$, while 4 atoms of W form 4^4 nets in the planes $z = 1/4$ and $3/4$ that center the columns of crossed octagons. The difference between $tI32$, which lacks 12 atoms of silicon, and $tI19$ is that in the latter, instead of 4^4 nets, a body-centered tetragonal substructure is embedded that is incommensurate with the framework of 48^2 nets.

The 3^2434 nets, which form the basis of the $oC16$ structure and of the incommensurate $tI11$ structure, are characteristic of AB_2 compounds.

In $CoGe_2$ $oC23$ [59], seven Co atoms are statistically distributed over eight positions. The Ge1 atoms form 3^2434 nets shifted relative to each other in the same way as they are in $oC16$. Between these nets, 4^4 nets are located, consisting of Ge2 atoms. The germanium 3^2434 and 4^4 nets alternate with 4^4 nets of Co atoms. If we remove the 4^4 nets of Ge2 atoms from the $CoGe_2$ structure and move the Co nets into the vacant positions in such a way that they form slightly corrugated $\sim 4^4$ nets, the structure becomes completely similar to $oC16$. The $PdSn_2$ $tI48$ structure can also be reduced to this structure [60].

One analog of the incommensurate structures $tI11$ is the $CuAl_2$ $tI12$ structure [61], in which the aluminum atoms produce two antisymmetric 3^2434 nets that form columns consisting of square antiprisms in the corners and at the center of the base of a tetragonal cell. The copper atoms form 4^4 nets arranged in the middle between the aluminum nets in such a way that the atoms in Cu chains center the antiprisms. Thus, the $tI11$ structures differ from this particular structure type of $CuAl_2$ in only one respect: the copper nets are replaced with incommensurate tetragonal substructures of different types.

The series of polymorphic transformations displayed in Fig. 1 show that, after undergoing several phase transitions in which the symmetry and the packing density are lowered, the crystal structures under sufficiently high pressures again become symmetric and close-packed: $cI2$ in As, Sb, and Bi; $hP3$ in Cs; and $hP3$ and $cF4$ in Si. It can be assumed that in these phases all the atoms again become identical and that alkali elements become d transition metals.

References

1. Tonkov E Yu *Fazovye Prevrashcheniya Soedinenii pri Vysokom Davlenii*: Spravochnik (High Pressure Phase Transformations: A Handbook) Vol. 1, 2 (Moscow: Metallurgiya, 1988) [Translated into English (Philadelphia: Gordon and Breach Sci. Publ., 1992)]
2. Young D A *Phase Diagrams of the Elements* (Berkeley: Univ. of California Press, 1991)
3. Nelmes R J, McMahon M I *J. Synchrotron Radiat.* **1** 69 (1994)
4. Rietveld H M *J. Appl. Crystallogr.* **2** 65 (1969)
5. Leigh G J (Ed.) *International Union of Pure and Applied Chemistry. Nomenclature of Inorganic Chemistry. Recommendations 1990* (Oxford: Blackwell Sci. Publ., 1990)
6. Pearson W B *The Crystal Chemistry and Physics of Metals and Alloys* (New York: Wiley-Intersci., 1972) Ch. 1–7 [Translated into Russian: Pt. 1 (Moscow: Mir, 1977)]
7. Brovman E G, Kagan Yu, Kholas A *Zh. Eksp. Teor. Fiz.* **61** 2429 (1971) [*Sov. Phys. JETP* **34** 1300 (1972)]
8. Brovman E G, Kagan Yu, Kholas A *Zh. Eksp. Teor. Fiz.* **62** 1492 (1972) [*Sov. Phys. JETP* **35** 783 (1972)]
9. Maksimov E G, Savrasov D Yu *Solid State Commun.* **119** 569 (2001)
10. Hanfland M et al. *Solid State Commun.* **112** 123 (1999)
11. Hanfland M et al. *Nature* **408** 174 (2000)
12. Takemura K, Syassen K *Solid State Commun.* **44** 1161 (1988)
13. Tups H, Takemura K, Syassen K *Phys. Rev. Lett.* **49** 1776 (1982)
14. Schwarz U et al. *Phys. Rev. Lett.* **83** 4085 (1999)
15. McMahon M I, Rekhi S, Nelmes R J *Phys. Rev. Lett.* **87** 055501 (2001)
16. Olijnyk H, Holzapfel W B *Phys. Lett. A* **99** 381 (1983)
17. Winzenick M, Vijayakumar V, Holzapfel W B *Phys. Rev. B* **50** 12381 (1994)
18. Schwarz U et al. *Solid State Commun.* **112** 319 (1999)
19. Hall H T, Merrill L, Barnett J D *Science* **146** 1297 (1964)
20. Takemura K, Minomura S, Shimomura O *Phys. Rev. Lett.* **49** 1772 (1982)
21. Schwarz U et al. *Phys. Rev. Lett.* **81** 2711 (1998)
22. Takemura K, Shimomura O, Fujihisa H *Phys. Rev. Lett.* **66** 2014 (1991)
23. Olijnyk H, Holzapfel W B *Phys. Lett. A* **100** 191 (1984)
24. Allan D R et al. *Rev. High Pressure Sci. Technol.* **7** 236 (1998)
25. McMahon M I et al. *Phys. Rev. B* **61** 3135 (2000)
26. Winzenick M, Holzapfel W B *Phys. Rev. B* **55** 101 (1997)
27. Takemura K *Phys. Rev. B* **50** 16238 (1994)
28. Nelmes R J et al. *Phys. Rev. Lett.* **83** 4081 (1999)
29. Hu J Z et al. *Phys. Rev. B* **34** 4679 (1986)
30. Duclos S J, Vohra Y K, Ruoff A L *Phys. Rev. Lett.* **58** 775 (1987)
31. Duclos S J, Vohra Y K, Ruoff A L *Phys. Rev. B* **41** 12021 (1990)
32. McMahon M I et al. *Phys. Rev. B* **50** 739 (1994)
33. Hanfland M et al. *Phys. Rev. Lett.* **82** 1197 (1999)
34. Beister H J, Strössner K, Syassen K *Phys. Rev. B* **41** 5535 (1990)
35. Greene R G, Luo H, Ruoff A L *Phys. Rev. B* **51** 597 (1995)
36. Degtyareva O, McMahon M I, Nelmes R J, in *Theses Intern. Workshop on Crystallography at High Pressure, Orsay, France, Sept. 4–8, 2001*
37. Kolobyanina T N et al. *Zh. Eksp. Teor. Fiz.* **59** 1146 (1970) [*Sov. Phys. JETP* **32** 624 (1971)]
38. Vereshchagin L F, Kabalkina S S *Rentgenostrukturnye Issledovaniya pri Vysokom Davlenii* (X-ray Structural Studies at High Pressure) (Moscow: Nauka, 1979) p. 98
39. McMahon M I, Degtyareva O, Nelmes R J *Phys. Rev. Lett.* **85** 4896 (2000)

40. Bragger R M, Bennion R B, Worlton T G *Phys. Lett. A* **24** 714 (1967)
41. Degtyareva V F *Phys. Rev. B* **62** 9 (2000)
42. Ahuja R, Eriksson O, Johansson B *Phys. Rev. B* **63** 14102 (2001)
43. Ahuja R, Eriksson O, Johansson B *Phys. Rev. B* **60** 14475 (1999)
44. Chang K J, Cohen M L *Phys. Rev. B* **31** 7819 (1985)
45. Louie S G, Cohen M L *Phys. Rev. B* **10** 3237 (1974)
46. McMahan A K *Phys. Rev. B* **29** 5982 (1984)
47. Schwarz U, Jepsen O, Syassen K *Solid State Commun.* **113** 643 (2000)
48. Aoki K, Fujiwara S, Kusakabe M *Solid State Commun.* **45** 161 (1983)
49. Iwasaki H, Kikegawa T *High Press. Res.* **6** 121 (1990)
50. Bridgman P W *Proc. Am. Acad. Arts Sci.* **74** 425 (1942)
51. Yamamoto A *Acta Crystallogr. A* **49** 831 (1993)
52. Bolotina N B et al. *Kristallogr.* **42** 972 (1997) [*Crystallogr. Rep.* **42** 896 (1997)]
53. Brouns E, Visser J W *Acta Crystallogr.* **17** 614 (1974)
54. Pearson W B *The Crystal Chemistry and Physics of Metals and Alloys* (New York: Wiley-Intersci., 1972) p. 570 [Translated into Russian: Pt. 2 (Moscow: Mir, 1977) p. 223]
55. Pearson W B *The Crystal Chemistry and Physics of Metals and Alloys* (New York: Wiley-Intersci., 1972) p. 565 [Translated into Russian: Pt. 2 (Moscow: Mir, 1977) p. 215]
56. Neaton J B, Ashcroft N W *Nature* **400** 141 (1999)
57. Swanson H E, Fuyat R K *NBS Circular* **539** 3 (1953)
58. Pearson W B *The Crystal Chemistry and Physics of Metals and Alloys* (New York: Wiley-Intersci., 1972) p. 732, Table 14-1 [Translated into Russian: Pt. 2 (Moscow: Mir, 1977) p. 386]
59. Pearson W B *The Crystal Chemistry and Physics of Metals and Alloys* (New York: Wiley-Intersci., 1972) p. 612 [Translated into Russian: Pt. 2 (Moscow: Mir, 1977) p. 264]
60. Pearson W B *The Crystal Chemistry and Physics of Metals and Alloys* (New York: Wiley-Intersci., 1972) p. 613 [Translated into Russian: Pt. 2 (Moscow: Mir, 1977) p. 266]
61. Pearson W B *The Crystal Chemistry and Physics of Metals and Alloys* (New York: Wiley-Intersci., 1972) p. 606 [Translated into Russian: Pt. 2 (Moscow: Mir, 1977) p. 258]